Research Article | Vol. 9, No. 7 | 1 Jul 2018 | BIOMEDICAL OPTICS EXPRESS 3284

Biomedical Optics EXPRESS

On the dysfunctional hemoglobins and cyanosis connection: practical implications for the clinical detection and differentiation of methemoglobinemia and sulfhemoglobinemia

STEPHEN W. ASKEW AND GLADIMIR V. G. BARANOSKI*

Natural Phenomena Simulation Group, D. R. Cheriton School of Computer Science, University of Waterloo, 200 University Avenue West, Waterloo, Ontario, Canada
*gvgbaran@curumin.math.uwaterloo.ca**

Abstract: Methemoglobinemia and sulfhemoglobinemia are potentially life-threatening blood-related disorders characterized by similar symptoms and markedly distinct treatment procedures. In this paper, we investigate the causal relationship between these conditions and the onset of cyanosis, which is typically associated with a purple or bluish skin coloration. More specifically, we perform controlled experiments to elicit cyanotic appearances resulting from different severity levels of these disorders and varying physiological conditions. We note that such experiments cannot be induced in living subjects without posing risks to their health. Accordingly, we have resorted to an *in silico* experimental approach supported by biophysical data reported in the literature. Besides bringing new insights about cyanotic chromatic variations elicited by methemoglobinemia and sulfhemoglobinemia, our investigation provides the basis for the proposition of a cost-effective protocol for the noninvasive detection and differentiation of these disorders. Our experimental results indicate that its sensitivity range is wider than what is provided by similar protocols employed in these tasks. Moreover, it has lower operational requirements than laboratory tests ordered to enable the diagnosis of these conditions. We believe that these aspects make the proposed protocol particularly suitable for deployment at the point of care of medical settings with limited access to laboratory resources.

OCIS codes: (170.0170) Medical optics and biotechnology; (170.1420) Biology; (170.1470) Blood or tissue constituent monitoring; (170.1610) Clinical applications; (170.4580) Optical diagnostics for medicine.

References and links

1. A. Baernstein, K. Smith, and J. Elmore, "Singing the blues: is it really cyanosis?" Resp. Care **53**, 1081–1084 (2008).
2. S. McMullen and W. Patrick, "Cyanosis," The American Journal of Medicine **126**, 210–212 (2013).
3. G. Baranoski, S. Van Leeuwen, and T. Chen, "Elucidating the biophysical processes responsible for the chromatic attributes of peripheral cyanosis," in *39th Annual International Conference of the IEEE Engineering in Medicine and Biology Society (EMBC)* (Jeju Island, South Korea, 2017), pp. 90–95.
4. L. Gharahbaghian, B. Massoudian, and G. Dimassa, "Methemoglobinemia and sulfhemoglobinemia in two pediatric patients after ingestion of hydroxylamine sulfate," West. J. Emerg. Med. **10**, 197–201 (2009).
5. C. Marple, "Cyanosis," The American Journal of Nursing **58**, 222–235 (1958).
6. G.Casey, "Oxygen transport and the use of pulse oxymetry," Nursing Standard **15**, 46–53 (2001).
7. R. Flewelling, "Noninvasive optical monitoring," in *The Biomedical Engineering Handbook*, 1st ed., J. D. Bronzino, ed. (CRC Press LLC, 1995), pp. 1346–1356.
8. S. Haymond, R. Cariappa, C. Eby, and M. Scott, "Laboratory assessment of oxygenation in methemoglobinemia," Clin. Chem. **51**, 434–444 (2005).
9. C. Lundsgaard and D. V. Slyke, "Cyanosis," in *Medicine Monographs* (Wlliams & Wilkins Company, The Rockfeller Institute for Medical Research, 1923), pp. 1–80.
10. A. George and D. Goetz, "A case of sulfhemoglobinemia in a child with chronic constipation," Resp. Med. Case Reports **21**, 21–24 (2017).
11. A. Gopalachar, V. Bowie, and P. Bharadwaj, "Phenazopyridine-induced sulfhemoglobinemia," Ann. Pharmacol. **39**, 1128–1130 (2005).
12. S. Guiducci and M. Matucci-Cerenic, "Definition, nomenclature and diagnostic criteria," in *Raynaud's Phenomenon, A Guide to Pathogenesis and Treatment*, F. M. Wigley, A. Herrick, and N. Flavahan, eds. (Springer, 2015), pp. 13–20.

#329038 https://doi.org/10.1364/BOE.9.003284
Journal © 2018 Received 26 Apr 2018; revised 5 Jun 2018; accepted 11 Jun 2018; published 25 Jun 2018

Biomedical Optics EXPRESS

13. C. Finch, "Methemoglobinemia and sulfhemoglobinemia," New England Journal of Medicine **239**, 470–478 (1948).
14. R. Smith, "The blue baby syndromes," American Scientist **97**, 94–96 (2009).
15. R. Ash-Bernal, R. Wise, and S. Wright, "Acquired methemoglobinemia A retrospective series of 138 cases at 2 teaching hospitals," Medicine **83**, 265–273 (2004).
16. S. Patnaik, M. Natarajan, E. James, and K. Ebenezer, "Methylene blue unresponsive methemoglobinemia," Indian J. Crit. Care Med. **18**, 253–255 (2014).
17. S. Zyoud, S. Al-Jabi, W. Sweileh, S. Al-Khalil, M. Alqub, and R. Awang, "Global methaemoglobinaemia research output (1940?2013): a bibliometric analysis," SpringerPlus **4**, 1–7 (2015).
18. J. Self and R. Waskom, "Nitrates in drinking water," in "Colorado State University Extension," (Colorado State University and U.S. Department of Agriculture, CO, USA, 2006). Fact Sheet 0.517, Crop Series, Soil.
19. G. Giangreco, D. Campbell, and M. Cowan, "A 32-year-old female with aids, *Pneumocystis jiroveci* pneumonia, and methemoglobinemia," Case Reports in Critical Care **2013**, 1–5 (2013).
20. L. Derbas, M. Warsame, M. Oma, Y. Zafar, and G. Howell, "Sulfhaemoglobinaemia caused by ferrous sulfate," BMJ Case Rep. **56**, 1–13 (2017).
21. K. Murphy, C. Ryan, E. Dempsey, P. W. Otoole, R. Ross, C. Stanton, and C. Ryan, "Neonatal sulfhemoglobinemia and hemolytic anemia associated with intestinal morganella morganii," Pediatrics **136**, e1641 (2015).
22. B. de Benoist, E. McLean, I. Egli, and M. Cogswell, eds., *Worldwide Prevalence of Anaemia 1993–2005 WHO Global Database on Anaemia* (World Health Organization, 2008).
23. S. El-Beshbishi, K. Shattuck, A. Mohammad, and J. Petersen, "Hyperbilirubinemia and transcutaneous bilirubinometry," Clin. Chem. **5**, 1280–1287 (2009).
24. P. Ginimuge and S. Jyothi, "Methylene blue: revisited," J. Anaesthesiol. Clin. Pharmacol. **26**, 517–520 (2010).
25. S. Shadnia, K. Soltaninejad, H. Hassanian-Moghada, A. Sadeghi, H. Rahimzadeh, N. Zamani, A. Ghasemi-toussi, and M. Abdollahi, "Methemoglobinemia in aluminium phosphide poisoning," Human and Experimental Toxicology **30**, 250–253 (2010).
26. G. Baranoski, T. Chen, B. Kimmel, E. Miranda, and D. Yim, "On the noninvasive optical monitoring and differentiation of methemoglobinemia and sulfhemoglobinemia," J. Biomed. Opt. **17**, 097005 (2012).
27. E. Wolak, F. Byerly, T. Mason, and B. Cairns, "Methemoglobinemia in critically ill burned patients," Am. J. Crit. Care **14**, 104–1018 (2005).
28. R. Peterson, K. Kadugodinandareddy, V. Karunakaran, C. Whitney, J. Ling, and J. Ye, "Utilizing an open-microcavity optoacoustic sensor for spectroscopic determination of methemoglobin concentration," in *SPIE BIOS, Optical Tomography and Spectroscopy of Tissue XI,* vol. 9319 (SPIE, 2015), pp. 93191N.
29. S. Van Leeuwen, G. Baranoski, and B. Kimmel, "Three-wavelength method for the optical differentiation of methemoglobin and sulfhemoglobin in oxygenated blood," in *39th Annual International Conference of the IEEE Engineering in Medicine and Biology Society (EMBC)* (Jeju Island, South Korea, 2017), pp. 4570–4573.
30. T. Karen, H. Bucher, and J. Fauchére, "Comparison of a new transcutaneous bilirubinometer (bilimed) with serum bilirubin measurments in preterm and full-term infants," BMC Pediatrics **9**, 1–7 (2009).
31. P. Szabo, M. Wolf, H. Bucher, D. Haensse, J. Fauchére, and R. Arlettaz, "Assessment of jaundice in preterm neonates: comparison between clinical assessment, two transcutaneous bilirubinometers and serum bilirubin values," Acta Paediatr. **93**, 1491–1495 (2004).
32. B. Harbrecht, M. Rsengart, K. Bubauskas, M. Zenati, J. Mrsh Jr., and D. Geller, "Assessment of transcutaneous bilirubinometry in hospitalized adults," J. Am. Coll. Surg. **206**, 1129–1136 (2008).
33. B. Ventura, C. Lemerle, K. Michalodimitrakis, and L. Serrano, "From *in vivo* to *in silico* biology and back," Nature **443**, 527–553 (2006).
34. M. Viceconti, A. Henney, and E. Morley-Fletcher, "In silico clinical trials: how computer simulation will transform the biomedical industry," Int. J. Clin. Trials **3**, 37–46 (2016).
35. V. Tuchin, *Tissue Optics: Light Scattering Methods and Instruments for Medical Diagnosis*, SPIE PM (SPIE/International Society for Optical Engineering, 2007).
36. T. Chen, G. Baranoski, B. Kimmel, and E. Miranda, "Hyperspectral modeling of skin appearance," ACM Trans. Graph. **34**(31), 1–14 (2015).
37. G. Baranoski and T. Chen, "Optical properties of skin surface," in *Agache's Measuring Skin*, vol. 1, P. Humbert, H. Maibach, F. Fanian, and P. Agache, eds. (Springer International Publishing, 2017), pp. 85–98.
38. G. Baranoski, J. Rokne, and G. Xu, "Virtual spectrophotometric measurements for biologically and physically-based rendering," The Visual Computer **17**, 506–518 (2001).
39. G. Baranoski, A. Dey, and T. Chen, "Assessing the sensitivity of human skin hyperspectral responses to increasing anemia severity levels," J. Biomed. Opt. **9**, 095002 (2015).
40. G. Baranoski, S. Van Leeuwen, and T. Chen, "On the detection of peripheral cyanosis in individuals with distinct levels of cutaneous pigmentation," in *39th Annual International Conference of the IEEE Engineering in Medicine and Biology Society (EMBC)*, (Jeju Island, South Korea, 2017), pp. 4260–4264.
41. S. Van Leeuwen and G. Baranoski, "Elucidating the contribution of Rayleigh scattering to the bluish appearance of veins," J. Biomed. Opt. **23**, 025001 (2018).
42. Natural Phenomena Simulation Group (NPSG), *Run HyLIoS Online*, School of Computer Science, University of Waterloo, Ontario, Canada (2017). http://www.npsg.uwaterloo.ca/models/hyliosEx.php.
43. G. Baranoski, T. Dimson, T. Chen, B. Kimmel, D. Yim, and E. Miranda, "Rapid dissemination of light transport

Biomedical Optics EXPRESS

models on the web," IEEE Comput. Graph. **32**, 10–15 (2012).
44. NPSG, *Human Skin Data*, Natural Phenomena Simulation Group (NPSG), School of Computer Science, University of Waterloo, Ontario, Canada (2014). http://www.npsg.uwaterloo.ca/data/skin.php.
45. Y. Yamaguchi, S. Itami, H. Watabe, K. Yasumoto, Z. A. Abdel-Malek, T. Kubo, F. Rouzaud, A. Tanemura, K. Yoshikawa, and V. Hearing, "Mesenchymal-epithelial interactions in the skin: increased expression of dickkopf1 by palmoplantar fibroblast inhibits melanocyte growth and differentiation," J. Cell Biol. **165**, 275–285 (2004).
46. R. Turner, G. Burch, and W. Sodeman, "Studies in the physiology of blood vessels in man. III. Some effects of raising and lowering the arm upon the pulse volume and blood volume of the human finger tip in health and in certain diseases of the blood vessels," J. Clin. Invest. **16**, 789–798 (1937).
47. C. Mignon, D. Tobin, M. Zeitouny, and N. Uzunbajakava, "Shedding light on the variability of optical skin properties: finding a path towards more accurate prediction of light propagation in human cutaneous compartments," Biomed. Opt. Express **9**, 852–872 (2018).
48. A. Caduff, M. Talary, and P. Zakharov, "Cutaneous blood perfusion as a perturbing factor for noninvasive glucose monitoring," Diabetes Technology & Therapeutics **12**, 1–9 (2010).
49. N. Hampson, C. Piantadosi, S. Thom, and L. Weaver, "Practice recommendations in the diagnosis, management, and prevention of carbon monoxide poisoning," Am. J. Resp. Crit. Care **186**, 1095–1101 (2012).
50. K. Jain, "Carbon monoxide and other tissue poisons," in *Textbook of Hyperbaric Medicine*, K. Jain, ed. (Springer International Publishing, 2017), pp. 131–154.
51. S. Cunnington A. J., Kendrick, B. Wamola, B. Lowe, and C. R. J. C. Newton, "Carboxyhemoglobin levels in kenyan children with plasmodium falciparum malaria," The American Journal of Tropical Medicine and Hygiene **71**, 43–47 (2004).
52. I. Yarynovska and A. Bilyi, "Absorption spectra of sulfhemoglobin derivatives of human blood," in *Optical Diagnostics and Sensing VI*, vol. 6094, G. Cote and A. Priezzhev, eds. (SPIE, 2006), pp. 1–6.
53. P. Talreja, G. Kasting, N. Kleene, W. Pickens, and T. Wang, "Visualization of the lipid barrier and measurement of lipid pathlength in human stratum corneum," AAPS PharmSci. **3**, 48–56 (2001).
54. N. Magnenat-Thalmann, P. Kalra, J. L. Leveque, R. Bazin, D. Batisse, and B. Querleux, "A computational skin model: fold and wrinkle formation," IEEE T. Inf. Technol. B. **6**, 317–323 (2002).
55. P. Agache, "Stratum corneum histophysiology," in "Measuring the Skin," P. Agache and P. Humbert, eds. (Springer-Berlag, 2004), pp. 95–100.
56. P. Agache, "Metrology of the stratum corneum," in *Measuring the Skin*, P. Agache and P. Humbert, eds. (Springer-Berlag, 2004), pp. 101–111.
57. G. Plewig, E. Scheuber, B. Reuter, and W. Waidelich, "Thickness of the corneocytes," in *Stratum Corneum*, R. Marks and G. Plewig, eds. (Springer-Verlag, 1983), pp. 171–174.
58. K. Robertson and J. Rees, "Variation in epidermal morphology in human skin at different body sites as measured by reflectance confocal microscopy," Acta Derm. Venereol. **90**, 368–373 (2010).
59. J. Whitton and J. Everall, "The thickness of the epidermis," British Journal of Dermatology **89**, 467–476 (1973).
60. M. Schwarz, M. Omar, A. Buehler, J. Aguirre, and V. Ntziachristos, "Implications of ultrasound frequency in optoacoustic mesoscopy of the skin," IEEE Trans. Med. Imaging **34**, 672–677 (2015).
61. R. Anderson and J. Parrish, "The optics of human skin," J. Investig. Dermatol. **77**, 13–9 (1981).
62. N. Kollias, R. Sayre, L. Zeise, and M. Chedekel, "Photoprotection by melanin," J. Photoch. Photobio. B. **9**, 135–60 (1991).
63. T. Lister, "Simulating the color of port wine stain skin," Ph.D. thesis, University of Southampton,U.K. (2013).
64. S. Alaluf, D. Atkins, K. Barret, M. Blount, N. Carter, and A. Heath, "Ethnic variation in melanin content and composition in photoexposed and photoprotected human skin," Pigment Cell Res. **15**, 112–118 (2002).
65. M. Pathak, "Functions of melanin and protection by melanin," in *Melanin: Its Role in Human Photoprotection*, M. C. L. Zeise and T. Fitzpatrick, eds. (Valdenmar Publishing Co., USA, 1995), pp. 125–134.
66. R. Olson, J. Gaylor, and M. Everett, "Skin color, melanin, and erythema," Arch. Dermatol. **108**, 541–544 (1973).
67. A. Thody, E. Higgins, K. Wakamatsu, S. Ito, S. Burchill, and J. Marks, "Pheomelanin as well as eumelanin is present in human epidermis," J. Investig. Dermatol. **97**, 340–344 (1991).
68. A. Hennessy, C. Oh, B. Diffey, K. Wakamatsu, S. Ito, and J. Rees, "Eumelanin and pheomelanin concentrations in human epidermis before and after UVB irradiation," Pigment Cell Res. **18**, 220–223 (2005).
69. G. Nilsson, T. Tenland, and P. Öberg, "Evaluation of a laser Doppler flowmeter for measuring of tissue blood flow," IEEE Transactions on Biomedical Engineering **27**, 597–604 (1980).
70. M. Noll and J. Byers, "Usefulness of measures of Svo_2, Spo_2, vital signs, and derived dual oximetry parameters as indicators of arterial blood gas variables during weaning of cardiac surgery patients from mechanical ventilation," Heart & Lung **24**, 220–227 (1995).
71. A. Yaroslavsky, A. Priezzhev, J. Rodriques, I. Yarolavsky, and H. Battarbee, "Optics of blood," in *Handbook of Optical Biomedical Engineering*, V. Tuchin, ed. (SPIE-Press, 2002), pp. 169–216.
72. S. Zucker, P. Horn, and K. Sherman, "Serum bilirubin levels in the US population: Gender effect and inverse correlation with colorectal cancer," Hepatology **40**, 827–835 (2004).
73. R. Lee, M. Mathews-Roth, M. Pathak, and J. Parrish, "The detection of carotenoid pigments in human skin," J. Investig. Dermatol. **64**, 175–177 (1975).
74. P. Agache, "Main skin biological constants," in *Measuring the Skin,* P. Agache and P. Humbert, eds. (Springer-Berlag,

Biomedical Optics EXPRESS

2004), pp. 727–746.
75. N. Nakagawa, M. Matsumoto, and S. Sakai, "*In vivo* measurement of the water content in the dermis by confocal Raman spectroscopy," Skin Research and Technology **16**, 137–141 (2010).
76. J. Viator, J. Komadina, L. Svaasand, G. Aguilar, B. Choi, and N. Stuart, "A comparative study of photoacoustic and reflectance methods for determination of epidermal melanin content," J. Investig. Dermatol. **122**, 1432–1439 (2004).
77. M. Williams, M. Hincenbergs, and K. Holbrook, "Skin lipid content during early fetal development," J. Investig. Dermatol. **91**, 263–268 (1988).
78. C. Squier, P. Cox, and P. Wertz, "Lipid content and water permeability of skin and oral mucosa," Journal of Investigative Dermatology **96**, 123–126 (1991).
79. A. Cerussi, A. Berger, F. Bevilacqua, N. Shah, D. Jakubowski, J. Butler, R. Holcombe, and B. J. Tromberg, "Sources of absorption and scattering contrast for near-infrared optical mammography," Academic Radiology **8**, 211–218 (2001).
80. E. Fuchs, "Keratins and the skin," Annual Review of Cell and Developmental Biology **11**, 123–154 (1995).
81. H. Shimizu, *Shimizu's Textbook of Dermatology* (Hokkaido University Press, 2007).
82. D. Gawkrodger and M. Ardern-Jones, *Dermatology An Illustrated Colour Text* (Churchill Livingstone, Elsevier, 2002), 3rd ed.
83. A. Young, "Chromophores in human skin," Phys. Med. Biol. **42**, 789 (1997).
84. J. Varcoe, *Clinical Biochemistry: Techniques and Instrumentation A Practical Course* (World Scientific, 2001).
85. R. Flindt, *Amazing Numbers in Biology* (Springer-Verlag, 2006).
86. G. Tearney, M. Brezinski, J. Southern, B. Bouma, M. Hee, and J. Fujimoto, "Determination of the refractive index of highly scattering human tissue by optical coherence tomography," Opt. Lett. **20**, 2258–2260 (1995).
87. B. Diffey, "A mathematical model for ultraviolet optics in skin," Phys. Med. Biol. **28**, 647–657 (1983).
88. S. Jacques, C. Alter, and S. Prahl, "Angular dependence of HeNe laser light scattering by human dermis," Lasers Life Sci. **1**, 309–333 (1987).
89. A. Bashkatov, E. Genina, V. Kochubey, and V. Tuchin, "Optical properties of human skin, subcutaneous and mucous tissues in the wavelength range from 400 to 2000 nm," J. of Physics D: Applied Physics **38**, 2543–2555 (2005).
90. X. Wang, T. Milner, and M. C. Chang, and J. S. Nelson, "Group refractive index measurement of dry and hydrated type I collagen films using optical low-coherence reflectometry," J. Biomed. Opt. **12**, 212–216 (1996).
91. S. Jacques, "Origins of tissue optical properties in the UVA, visible, and NIR regions," OSA TOPS on Adv. in Opt. Imaging and Photon Migration **2**, 364–369 (1996).
92. R. Hunt, *Measuring Colour* (Ellis Horwood Limited, 1991), 2nd ed.
93. S. Askew, "On skin cyanotic appearances and spectral responses elicited by methemoglobinemia and sulfhemoglobinemia," Master's thesis, D.R. Cheriton School of Computer Science, University of Waterloo (2018).
94. G. Baranoski and A. Krishnaswamy, *Light & Skin Interactions: Simulations for Computer Graphics Applications* (Morgan Kaufmann/Elsevier, Burlington, MA, USA, 2010).
95. M. Stokes, M. Fairchild, and R. Berns, "Precision requirements for digital color reproduction," ACM Trans. Graph. **11**, 406–422 (1992).
96. D. Brainard, "Color appearance and color difference specification," The Science of Color **2**, 191–216 (2003).
97. D. Yim, G. Baranoski, B. Kimmel, T. Chen, and E. Miranda, "A cell-based light interaction model for human blood," Computer Graphics Forum **31**, 845–854 (2012).
98. G. B. Thomas, R. Finney, and M. Weir, *Calculus and Analytic Geometry*, 9th ed. (Addison-Wesley Publishing Company, 1996).
99. C. Gerald and P. Wheatley, *Applied Numerical Analysis*, 5th ed. (Addison-Wesley Publishing Company, 1999).
100. D. Judd and G. Wyszecki, *Color in Business, Science and Industry* (John Wiley & Sons, 1975), 3rd ed.
101. G. Zerlaut and T. Anderson, "Multiple-integrating sphere spectrophotometer for measuring absolute spectral reflectance and transmittance," Applied Optics **20**, 3797–3804 (1981).
102. O. Siggaard-Andersen, B. Nrgaard-Pedersen, and J. Rem, "Hemoglobin pigments. spectrophotometric determination of oxy-, carboxy-, met-, and sulfhemoglobin in capillary blood," Clinica Chimica Acta **42**, 85–100 (1972).
103. L. Randeberg, J. Bonesrønning, M. Dalaker, J. Nelson, and L. Svaasand, "Methemoglobin formation during laser induced photothermolysis of vascular skin lesions," Lasers in Surgery and Medicine **34**, 414–419 (2004).

1. Introduction

A number of medical conditions, including arterial thrombosis and heart failure, can have as one their most noticeable initial symptoms cyanosis [1–3], a characteristic purple or bluish coloration of the skin (Fig. 1), nail beds and mucosal membranes. In its early stages, it can also appear as a grey cutaneous discoloration [4]. Although cyanosis is often elicited by the presence of high levels of deoxygenated hemoglobin in the blood-perfused dermal tissues [5, 6], it can also be elicited by other factors. These include the presence of abnormal amounts of dysfunctional forms of hemoglobin (which are characterized by not having the capability to bind reversibly with oxygen [7, 8]) in these tissues [3]. In this case, cyanosis is associated with the occurrence of two

Biomedical Optics EXPRESS

Fig. 1. Photograph showing hands depicting a cyanotic appearance [12], notably on the fingertips. It can be a symptom of a number of medical conditions, from a disorder of the blood vessels (as it is the case for this patient) known as Raynaud's phenomenon [12] to disorders affecting the blood's capability to transport oxygen known as methemoglobinemia and sulfhemoglobinemia. Reprinted by permission from Springer.

blood-related disorders known as methemoglobinemia and sulfhemoglobinemia [5, 8–11].

Methemoglobinemia is mostly caused by exposure to chemical agents that oxidize the iron atom in the hemoglobin molecule, turning it into a dysfunctional form of hemoglobin known as methemoglobin (MetHb) [13, 14]. Among the chemical agents leading to this altered form of hemoglobin, one can highlight drugs used in hospitals and outpatient settings such as local anesthetics (*e.g.*, benzocaine and lidocaine) and anti-infectives (*e.g.*, sulfonamide and sulfoxone) [15–17], as well as substances, such as nitrates present in fertilizers [14, 18], that may contaminate food and water supplies [14, 19]. The reader interested in a comprehensive review of these chemical agents is referred to the works by Ash-Bernal *et al.* [15] and Giangreco *et al.* [19].

Sulfhemoglobinemia has been associated with the exposure to sulfides whose sulfur atom can be incorporated into a hemoglobin molecule, turning it into a dysfunctional form of hemoglobin known as sulfhemoglobin (SHb) [5, 13]. Although the chemical agents that may lead to sulfhemoglobinemia have not been as extensively mapped as those causing methemoglobinemia, it has been observed [20] that some of the compounds that cause the latter can cause the former, including over-the-counter drugs (*e.g.*, phenazopyridine). In addition, it has been reported in patients taking sulphur-based medications or who have cultured sulfide-producing intestinal bacteria such as *Morganella morgani* [10, 21] .

The clinical relevance of detecting and differentiating methemoglobinemia and sulfhemoglobinemia spans from two facts. First, these dyshemoglobinemia disorders, albeit not as prevalent as other blood-related conditions (*e.g.*, anemia [22] and hyperbilirubinemia [23]) can be acquired by a patient in a relatively ordinary manner as briefly outlined above. Hence, their incidence should not be overlooked. For example, Ash-Bernal *et al.* [15] have reported 128 cases of methemoglobinemia at two teaching hospitals in a period of 28 months. Second, these disorders can rapidly escalate to a life-threatening situation if they are not treated promptly [5, 8, 10].

Methemoglobinemia and sulfhemoglobinemia are characterized by similar symptoms, which worsen as the MetHb and SHb levels increase [4, 8]. Both can lead to hypoxemia (abnormally low level of oxygen in the blood) and result in end-organ damage and death due to oxygen deprivation [4, 10, 19–21]. In the case of methemoglobinemia, a high mortality rate is often observed when the MetHb level is superior to 70% of the total hemoglobin content [8]. In the case of sulfhemoglobinemia, end-organ damage and death can occur when the SHb level is superior to 60% of the total hemoglobin content [4, 10]. It is important note that, to the best of our knowledge, the existing literature on these disorders lacks statistical studies quantitatively addressing their incidence and mortality rates.

In most cases, methemoglobinemia is reversible through the administration of a substance

Biomedical Optics EXPRESS

known as methylene blue [24]. There have been reports, however, of unusual cases in which it did not respond to this treatment [16, 25]. Unlike MetHb, SHb cannot be reconverted to functional hemoglobin and it lasts the lifetime of a red blood cell. Thus, sulfhemoglobinemia is not reversible and its management often requires blood transfusions which may pose additional risks to the patient [4, 26]. Accordingly, if sulfhemoglobinemia is misdiagnosed as methemoglobinemia, which can happen due to the similarity of their symptoms [4, 8], the use of methylene blue as antidote will be ineffective [20]. In addition, it may lead to other medical problems such as renal failure [27]. These aspects highlight the importance of the early detection and differentiation of these dyshemoglobinemia disorders.

Devices like co-oximeters and blood gas analyzers can be employed to detect the abnormal presence of MetHb and SHb in blood samples [10, 19]. There are, however, two aspects that need to be examined when considering this approach, namely cost and effectiveness. With respect to cost limitations, it worth noting that these detection tests are not performed routinely in most intensive care units and need to be ordered specifically [19]. Hence, one can expect their availability to be even more limited in low-resource clinical settings. Moreover, their use requires a high degree of expertise, which also increases their operational costs [4].

With respect to effectiveness, it has been reported that the readings provided by these devices can diverge significantly from actual MetHb and SHb values [10, 20, 21]. Moreover, available co-oximeters often have difficulties to differentiate between SHb and MetHb [20, 26]. In fact, SHb is often erroneously detected as MetHb by these devices, resulting in a false-positive diagnosis for methemoglobinemia [4, 21]. For example, in a recent report by Derbas *et al.* [20], the authors stated that the readings provided by a blood gas analyser resulted in a false-positive diagnosis for methemoglobinemia in a patient subjected to sulfhemoglobinemia whose blood samples contained a small level of MetHb (2%). Most blood gas analysers, on the other hand, typically do not report SHb levels [20]. Again, it is worth noting that, to the best of our knowledge, the existing literature on these disorders still lacks more comprehensive quantitative analyses about the effectiveness of these devices despite the relevant efforts of several research groups such as those whose works are cited above.

Other technologies, such as the use of optoacoustic sensors [28] or dedicated spectral sensors [29], have been proposed to detect the presence of dysfunctional hemoglobins in the blood stream. However, they also depend on the collection of blood samples. This invasive procedure may be not only painful, notably for infants [14, 30], but it may also result in undesirable situations. These may include, for example, a significant blood loss if multiple blood samples need to be collected. Such a situation may be particularly worrisome in the case of preterm infants [30]. In addition, it is worth noting that the possibility of contamination exists when one performs an invasive procedure. On the other hand, such a possibility, by definition, can be ruled out when the procedure being performed is noninvasive. In fact, these aspects have also motivated the development of noninvasive procedures for the detection and assessment of other blood-related disorders such as hyperbilirubinemia (*e.g.*, [30–32]).

Ideally, one would like to employ noninvasive and low-cost approaches in the detection and differentiation of methemoglobinemia and sulfhemoglobinemia, particularly at the point-of-care. These include the visual assessment of cyanosis [26]. However, the extent to which this assessment can contribute for the effective detection and differentiation of these disorders remains an open problem. This can be largely attributed to the relatively limited amount of experimental information about the impact of different levels of MetHb and SHb on skin appearance available in the literature. Oftentimes, works relating cyanosis to abnormal levels of MetHb and SHb refer to *in vitro* experiments performed considering only a handful of test cases [10]. In fact, the scarcity of comprehensively reported cases (that include relevant chromatic and/or spectral data related to the onset of cyanotic skin appearances elicited by these disorders) represents a major obstacle for advances in this area [10, 19, 21, 26]. Besides these data limitations, controlled *in vivo*

Biomedical Optics EXPRESS

quantitative investigations of cyanosis caused by dyshemoglobinemia disorders would involve a relatively large number of biophysical parameters that would need to be kept fixed during the experiments. This would represent another technical challenge.

Nowadays, controlled *in silico* experiments performed through predictive computer simulations are being extensively employed in biomedical research [33, 34]. In the specific case of light interactions with human skin, the information derived from *in silico* experiments contributes not only to the elucidation of scientific questions about these phenomena, but also to the development of more effective procedures aimed at the noninvasive diagnosis and treatment of diseases [26,35]. Besides its flexibility and the absence of the health-related risks normally associated with *in vivo* experiments, such an investigation approach mitigates the impact of the technical constraints mentioned above. For example, a larger number of diverse experiments can be carried out *in silico* since they are not bound by equipment constraints and/or subjects' availability. In addition, specific biophysical parameters of interest can be varied while the remaining ones can be simply treated as constants during the simulations.

For these reasons, we also resorted to an *in silico* approach in the work described in this paper. More precisely, we performed controlled *in silico* experiments to closely investigate the impact of key biophysical factors on the onset of cyanosis elicited by methemoglobinemia and sulhemoglobinemia. Our findings, in addition to broadening the current knowledge about this complex causal relationship, enabled us to propose a cost-effective protocol for the noninvasive detection and differentiation of these life-threatening disorders. The proposed protocol is expected to outperform the existing technologies available to carry out these tasks, notably in terms of sensitivity range and operational overhead.

The remainder of this paper is organized as follows. In Section 2, we describe the methods and data employed in this investigation. In Section 3, we present our findings, discuss their practical implications and propose a protocol for the noninvasive detection and differentiation of methemoglobinemia and sulfhemoglobinemia. Finally, in Section 4, we conclude the paper and comment on future prospects in this area.

2. Methods and data

In this investigation, we performed controlled *in silico* experiments considering distinct severity levels of methemoglobinemia and sulfhemoglobinemia. More specifically, we used a predictive model of light and skin interactions (Section 2.1) and specimen characterization data provided in the literature (Section 2.2) to compute directional-hemispherical reflectance curves for a cutaneous site considering variations in its dysfunctional hemoglobins (MetHb and SHb) levels and blood content. We then generate skin swatches (Section 2.3) to analyze the visual differences between the cyanotic appearances elicited by these disorders.

2.1. In silico experimental set-up

The model employed in our controlled *in silico* experiments, known as HyLIoS (*H*yperspectral *L*ight *I*mpingement on *S*kin) [36], employs a first-principles simulation approach. Accordingly, it accounts for all main light absorbers (keratin, DNA, uranic acid, eumelanin, pheomelanin, hemoglobins (functional and dysfunctional forms), beta-carotene, bilirubin, lipids and water) and scatterers (cells, fibers, fibrils, melanosomes and melanosome complexes) acting within the cutaneous tissues [37]. These correspond to the stratum corneum, the melanin-containing epidermis (subdivided into three main layers, the stratum granulosum, the stratum spinosum and the stratum basale) and the blood-perfused dermis (subdivided into a thin papillary layer and a dominant reticular layer).

Within the HyLIoS' geometrical-optics formulation, a ray interacting with a given skin specimen can be associated with any wavelength within a spectral region of interest. For consistency, we considered a spectral resolution of 5 *nm* in all curves depicted in this work, which

Biomedical Optics EXPRESS

were computed using a virtual spectrophotometer [38]. In their computation, we employed 10^6 sample rays and, unless otherwise stated, considered an angle of incidence equal to 15°.

Clearly, the reliability of an *in silico* experimental framework is directly associated with the predictive capabilities of the computer model used in the simulations. Hence, it is important to note that HyLIoS was extensively evaluated through qualitative and quantitative comparisons of its outcomes with actual measured data [36]. Since then, it has been effectively employed in a number of related biomedical investigations (*e.g.*, [3, 39–41]).

For conciseness, we refer the reader interested in the full description of the HyLIoS model to the publication in which it was originally presented [36]. Moreover, for the readers interested in the full reproduction of our *in silico* experimental results, we note that HyLIoS is available online [42] via a model distribution system [43] along with the supporting data (*e.g.*, refractive index and extinction coefficient curves of the light absorbers) [44] used in our investigation. This system enables researchers to specify the values to be assigned to the measurement variables (*e.g.*, angle of incidence and spectral range) and specimen characterization parameters (Tables 1, 2 and 3) using a web interface [42], and receive customized simulation results.

2.2. Specimen characterization data

We have elected the palmar fingertip as the testing site for our *in silico* experiments for the following reasons. This hypopigmented site is characterized by a reduced melanin content (more than fivefold lower than in the nonpalmoplantar sites [45]), which minimizes the masking effects of melanin on the visual assessment of cyanotic appearances [19, 40]. In addition, it is also characterized by an increased blood content [40, 46], making their spectral responses, and consequently, their cyanotic chromatic attributes more susceptible to changes in the levels of blood-borne pigments like MetHb and SHb. It is worth noting that the noninvasive measurement of blood related properties (*e.g.*, oxygen saturation levels measured using a pulse oximeter [7]) is usually performed at this site, which has also been considered in previous investigations involving peripheral cyanosis [3, 40].

Without loss of generality, we have characterized a palmar fingertip site in its normal (baseline) state using the dataset presented in Table 1. The selection of values for the parameters included in this dataset was based on physiologically valid ranges provided in related references, which are also listed in Table 1. Clearly, the use of parameter values outside physiologically valid ranges is detrimental to the reliability of findings derived from computer simulations. We note that, for some of the parameters listed in Table 1, the determination of physiologically valid ranges involved the use of multiple references. This was necessary due to the variability [47] in the values reported for some of these parameters in the literature.

Using HyLIoS and the dataset provided in Table 1, we then computed the baseline reflectance curve (Fig. 2(b)) used as reference in our experiments. Subsequently, we computed reflectance curves associated with distinct severity levels of methemoglobinemia and sulfhemoglobinemia using modified versions of this dataset. These modified versions correspond to the dataset provided in Table 1, with the MetHb, SHb and functional hemoglobin (Hb) concentrations in blood replaced by the values provided in Tables 2 and 3. We remark that these disorders are associated with the abnormal presence of MetHb and SHb in the blood stream. Hence, in our experiments, we also took into account variations in the blood content of the reticular dermis (denoted by v^{rd}_{blood}) from 2% to 15% [48].

In our baseline case, we considered MetHb, COHb (another type of dysfunctional hemoglobin, known as carboxyhemoglobin, not associated with cyanotic appearances [49, 50]) and SHb concentrations in blood equal to 1.5, 1.5 and 0 g/L. It is worth noting that this selection of values was performed considering that, in normal physiological states, only small traces ($< 2\%$) of COHb and MetHb are found in human blood [8, 51, 52], while SHb is absent [4, 52].

Biomedical Optics EXPRESS

Table 1. Parameters employed in the characterization of a palmar fingertip. The acronyms SC, SG, SS, SB, PD and RD refer to the skin layers considered by HyLIoS: stratum corneum, stratum granulosum, stratum spinosum, stratum basale, papillary dermis and reticular dermis, respectively.

Parameter	Value	Ref.
Ratio of Skin Surface Folds	0.1	[53] [54]
SC Thickness (cm)	0.013	[55] [56] [57] [58]
SG Thickness (cm)	0.0123	[59]
SS Thickness(cm)	0.0123	[59]
SB Thickness (cm)	0.0123	[59]
PD Thickness (cm)	0.02	[60]
RD Thickness (cm)	0.125	[61]
SC Melanosome Content (%)	0.0	[62] [63]
SG Melanosome Content (%)	0.0	[62] [63]
SS Melanosome Content (%)	0.0	[62] [63]
SB Melanosome Content (%)	0.15	[52]
SC Colloidal Melanin Content (%)	0.06	[62] [64] [65]
SG Colloidal Melanin Content (%)	0.06	[62] [64] [65]
SS Colloidal Melanin Content (%)	0.06	[62] [64] [65]
SB Colloidal Melanin Content (%)	0.06	[52]
SB Melanosome Dimensions ($\mu m \times \mu m$)	0.41×0.17	[66]
Melanosome Eumelanin Concentration (g/L)	32.0	[67] [68]
Melanosome Pheomelanin Concentration (g/L)	2.0	[67] [68]
PD Blood Content (%)	0.5	[48]
RD Blood Content (%)	2.0	[69]
Dermal Oxygenated Hemoglobin Fraction (%)	90.0	[70]
Functional Hemoglobin Concentration in Blood (g/L)	147.0	[71]
Blood Bilirubin Concentration (g/L)	0.003	[72]
SC Beta-Carotene Concentration (g/L)	2.1E-4	[73]
Epidermis Beta-Carotene Concentration (g/L)	2.1E-4	[73]
Blood Beta-Carotene Concentration (g/L)	7.0E-5	[73]
SC Water Content (%)	35.0	[74] [75]
Epidermis Water Content (%)	60.0	[74] [76]
PD Water Content (%)	75.0	[74] [76]
RD Water Content (%)	75.0	[74] [76]
SC Lipid Content (%)	20.0	[77]
Epidermis Lipid Content (%)	15.1	[74] [78] [79]
PD Lipid Content (%)	17.33	[74] [78] [79]
RD Lipid Content (%)	17.33	[74] [78] [79]
SC Keratin Content (%)	65.0	[80] [81] [82]
SC Urocanic Acid Density (mol/L)	0.01	[83]
Skin DNA Density (g/L)	0.185	[74] [84] [85]
SC Refractive Index	1.55	[86] [87]
Epidermis Refractive Index	1.4	[35] [54]
PD Refractive Index	1.39	[86] [88]
RD Refractive Index	1.41	[86] [88]
Melanin Refractive Index	1.7	[89]
PD Scatterers Refractive Index	1.5	[90]
Radius of PD Scatterers (nm)	40.0	[69]
PD Fraction Occupied by Scatterers (%)	22.0	[91]

Biomedical Optics EXPRESS

Table 2. MetHb and functional hemoglobin concentrations (in g/L) used in the simulation of distinct severity levels (represented by percentages of MetHb with respect to total hemoglobin content) of methemoglobinemia.

	10%	20%	30%	40%	50%	60%	70%	80%
MetHb	15	30	45	60	75	90	105	120
Functional Hemoglobins	133.5	118.5	103.5	88.5	73.5	58.5	43.5	28.5

Table 3. SHb and functional hemoglobin concentrations (in g/L) used in the simulation of distinct severity levels (represented by percentages of SHb with respect to total hemoglobin content) of sulfhemoglobinemia.

	10%	20%	30%	40%	50%	60%	70%	80%
SHb	15	30	45	60	75	90	105	120
Functional Hemoglobins	132	117	102	87	72	57	42	27

2.3. Swatch generation and analysis

Our investigation also included the generation of skin swatches, henceforth referred to as MetHb and SHb swatches, to enable the analysis of the visual impact of distinct severity levels of methemoglobinemia and sulfhemoglobinemia, respectively, on cyanotic appearances elicited by these disorders. The swatches' chromatic attributes (represented as RGB triples) were obtained from the convolution of a selected illuminant's relative spectral power distribution, the modeled reflectance data and the broad spectral response of the human photoreceptors [92]. This last step was performed [93] by employing a standard CIEXYZ to sRGB color system conversion procedure [94] and considering the CIE standard D65 (daylight) illuminant [92] (Fig. 2(a)). After computing the chromatic attributes of a swatch, we applied a greyscale texture (Fig. 2(c)) to make its depiction more realistic. For comparison purposes, the skin swatch obtained using the baseline reflectance curve (Fig. 2(b)) computed for the selected specimen is presented in (Fig. 2(d)).

Besides visual inspection, we also employed a device-independent CIE-based metric to compare skin swatches associated with distinct severity levels of methemoglobinemia and sulfhemoglobinemia. More specifically, we computed the CIELAB differences between pairs of swatches using the following formula [95]:

$$\Delta E^*_{ab} = \sqrt{{d_L}^2 + {d_a}^2 + {d_b}^2}, \tag{1}$$

where d_L, d_a and d_b represent the differences $L^*_1 - L^*_2$, $a^*_1 - a^*_2$ and $b^*_1 - b^*_2$, respectively, in which L^*, a^* and b^* correspond to the CIELAB color space dimensions. These are calculated for the modeled chromatic attributes (RGB triples) associated with the compared swatches (indicated by the subscripts 1 and 2, respectively). Again, we performed these calculations [93] using standard formulas employed in colorimetry [96] and considering the CIE standard D65 illuminant [92]. For the interested reader, we note that the RGB triples associated with each pair of compared MetHb and SHb swatches are provided elsewhere for conciseness [93].

3. Results and discussion

In this section, we present our findings and discuss their practical implications for the differentiation and monitoring of methemoglobinemia and sulfhemoglobinemia. We start with the examination of the reflectance curves obtained in our *in silico* experiments, henceforth referred to as dysfunctional (MetHb or SHb) reflectance curves, followed by a visual inspection and analysis of appearance

Biomedical Optics EXPRESS

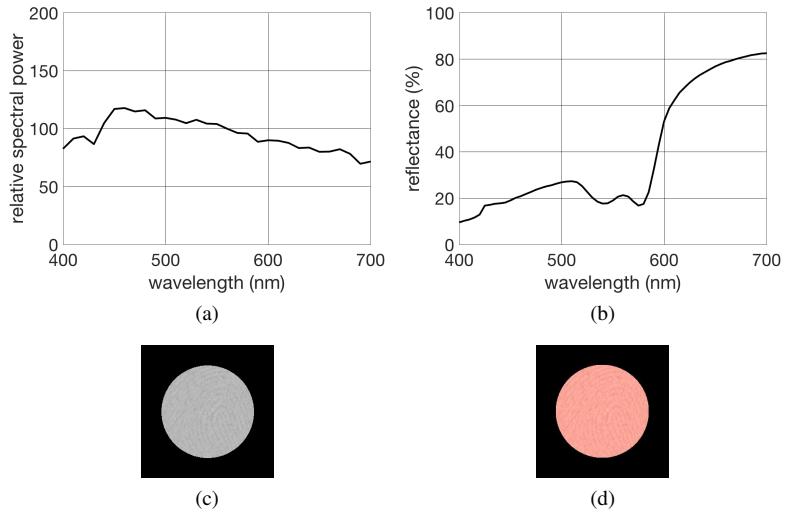

Fig. 2. Components of the convolution process employed to generate a skin swatch depicting a palmar fingertip in its normal (baseline) state. (a) The relative spectral power distribution of the CIE standard D65 illuminant. (b) The baseline reflectance curve computed using the parameter values depicted in Table 1. (c) Greyscale texture of a palmar fingertip. (d) Resulting swatch.

changes resulting from distinct severity levels of methemoglobinemia and sulfhemoglobinemia. Building on the observations derived from our *in silico* experimental results, we then outline a cost-effective protocol for the noninvasive detection and differentiation of methemoglobinemia and sulfhemoglobinemia.

3.1. Methemoglobinemia and sulfhemoglobinemia spectral responses

Initially, we performed experiments considering the blood content of the reticular dermis (v^{rd}_{blood}) equal to 2%. The results of these experiments are depicted in the graphs presented in Fig. 3. By examining these graphs, one can observe that the deviation of the dysfunctional reflectance curves from the baseline reflectance curve (Fig. 2(b)) becomes more pronounced as the presence of MetHb and SHb increases, albeit with distinct deviation patterns being observed for the MetHb and SHb curves. More precisely, in the "blue" region (400 to 500 *nm*) of the visible light spectrum, one can observe a decrease in the MetHb curves and an increase in the SHb curves. In the "green" region (500 to 600 *nm*), one can observe an increase in both sets of curves. This increase, however, is more prominent for the SHb curves. As a consequence, these curves show a more pronounced deviation from the characteristic "w" shape (associated with a dominant presence of oxygenated hemoglobin [97]) present in the baseline reflectance curve (Fig. 2(b)). Finally, in the "red" region (600 to 700 *nm*), one can observe a decrease in both sets of curves. This decrease, however, is again more prominent for the SHb curves.

Afterwards, we performed experiments considering v^{rd}_{blood} equal to 5%, 10% and 15%, whose results are presented in Figs. 4 to 6, respectively. Although the same deviation patterns noted for the 2% case can be observed for the 5%, 10% and 15% cases, the differences between the MetHb and SHb curves become smaller as v^{rd}_{blood} increases, particularly in the "blue" and "green" regions. In the "red" region, while both sets of curves become closer in the 600 to 650 *nm* interval, they remain relatively far apart in 650 to 700 *nm* interval. This can be explained by the relatively low absorption of light by both MetHb and SHb in this interval [26]. Thus, an increase in blood content will have a negligible impact on the reflectance values within this interval.

Biomedical Optics EXPRESS

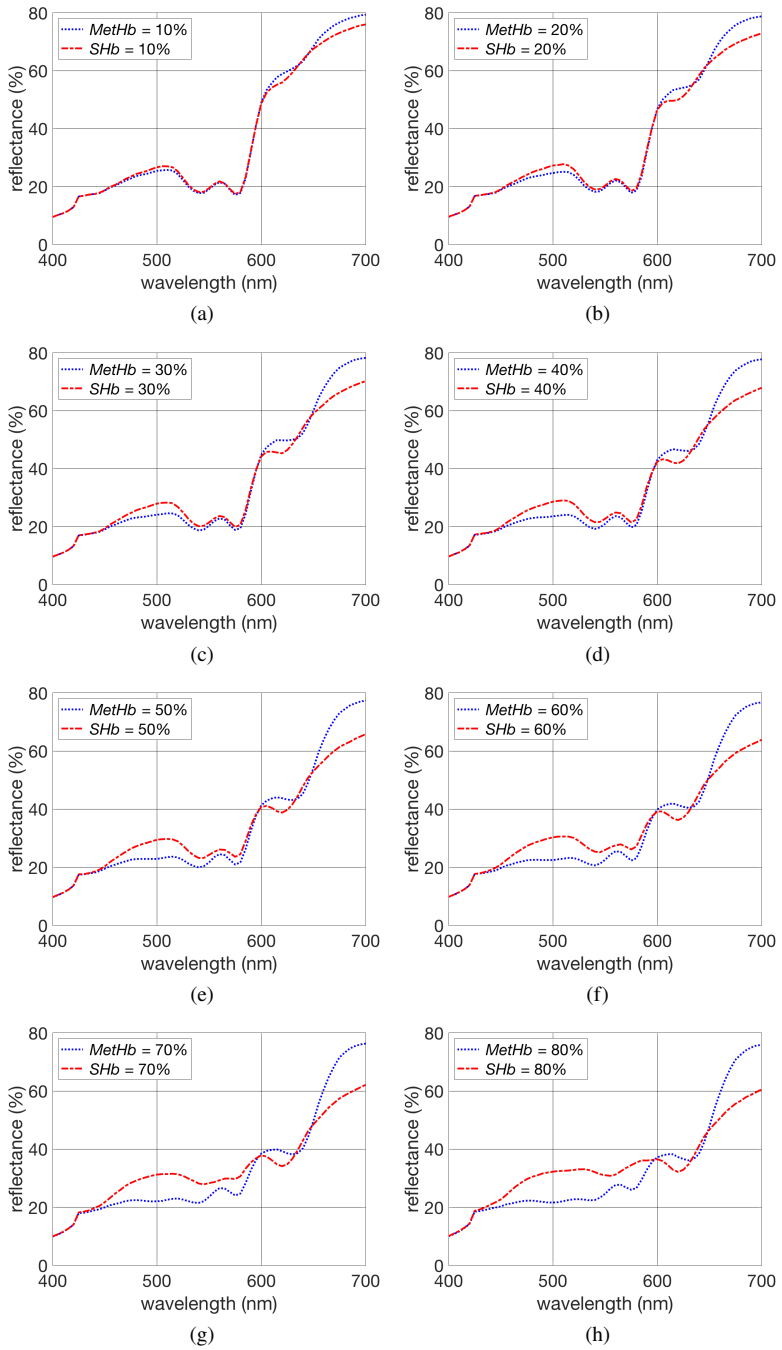

Fig. 3. Graphs depicting reflectance curves resulting from increasing amounts of methemoglobin (MetHb) and sulfhemoglobin (SHb) in a skin specimen characterized by a reticular blood content (v_{blood}^{rd}) equal to 2%. These curves were obtained using the HyLIoS [36] model and considering an angle of incidence equal to 15°. Each graph corresponds to a distinct severity level of methemoglobinemia and sulfhemoglobinemia: (a) 10%, (b) 20%, (c) 30%, (d) 40%, (e) 50%, (f) 60%, (g) 70% and (h) 80%. The concentrations of dysfunctional and functional hemoglobins associated with these levels are provided in Tables 2 and 3. The remaining parameters values used in the specimen's characterization are provided in Table 1.

Biomedical Optics EXPRESS

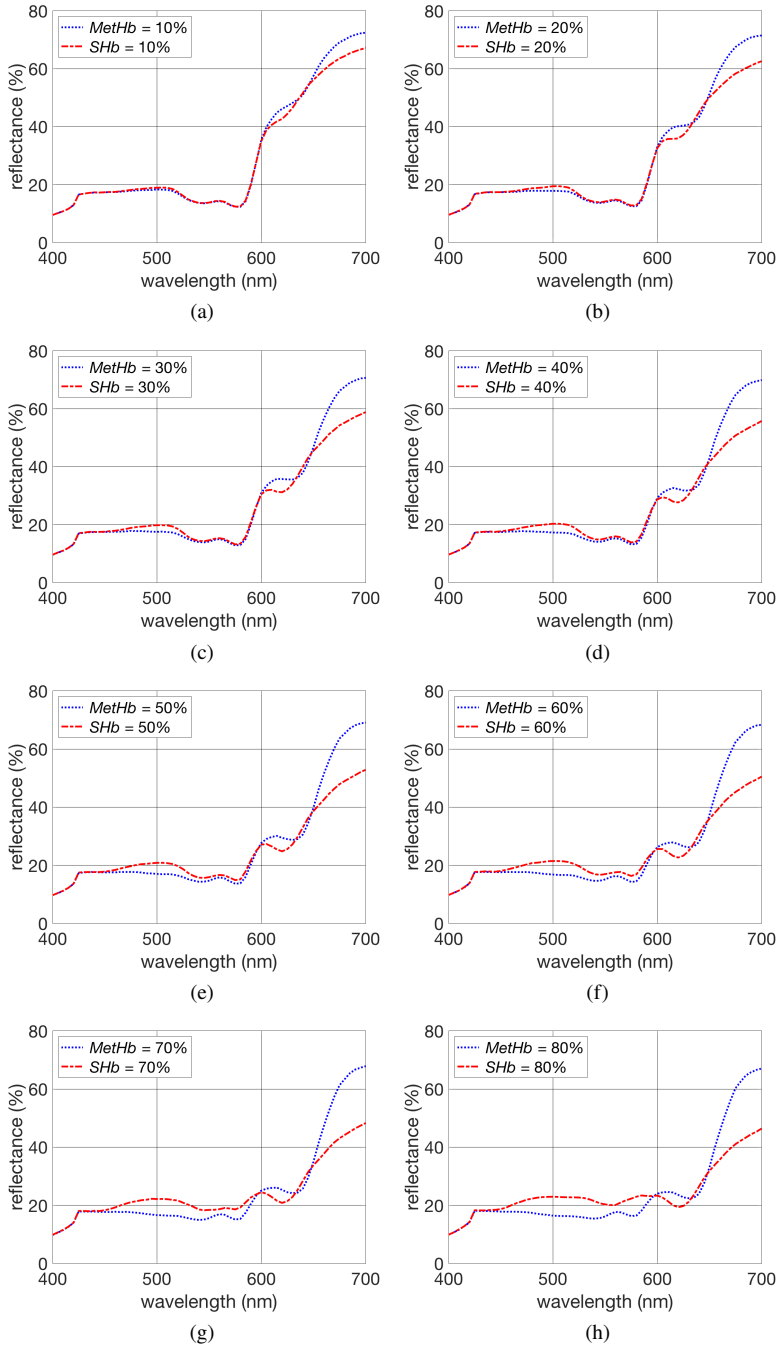

Fig. 4. Graphs depicting reflectance curves resulting from increasing amounts of methemoglobin (MetHb) and sulfhemoglobin (SHb) in a skin specimen characterized by a reticular blood content (v_{blood}^{rd}) equal to 5%. These curves were obtained using the HyLIoS [36] model and considering an angle of incidence equal to 15°. Each graph corresponds to a distinct severity level of methemoglobinemia and sulfhemoglobinemia: (a) 10%, (b) 20%, (c) 30%, (d) 40%, (e) 50%, (f) 60%, (g) 70% and (h) 80%. The concentrations of dysfunctional and functional hemoglobins associated with these levels are provided in Tables 2 and 3. The remaining parameters values used in the specimen's characterization are provided in Table 1.

Biomedical Optics EXPRESS

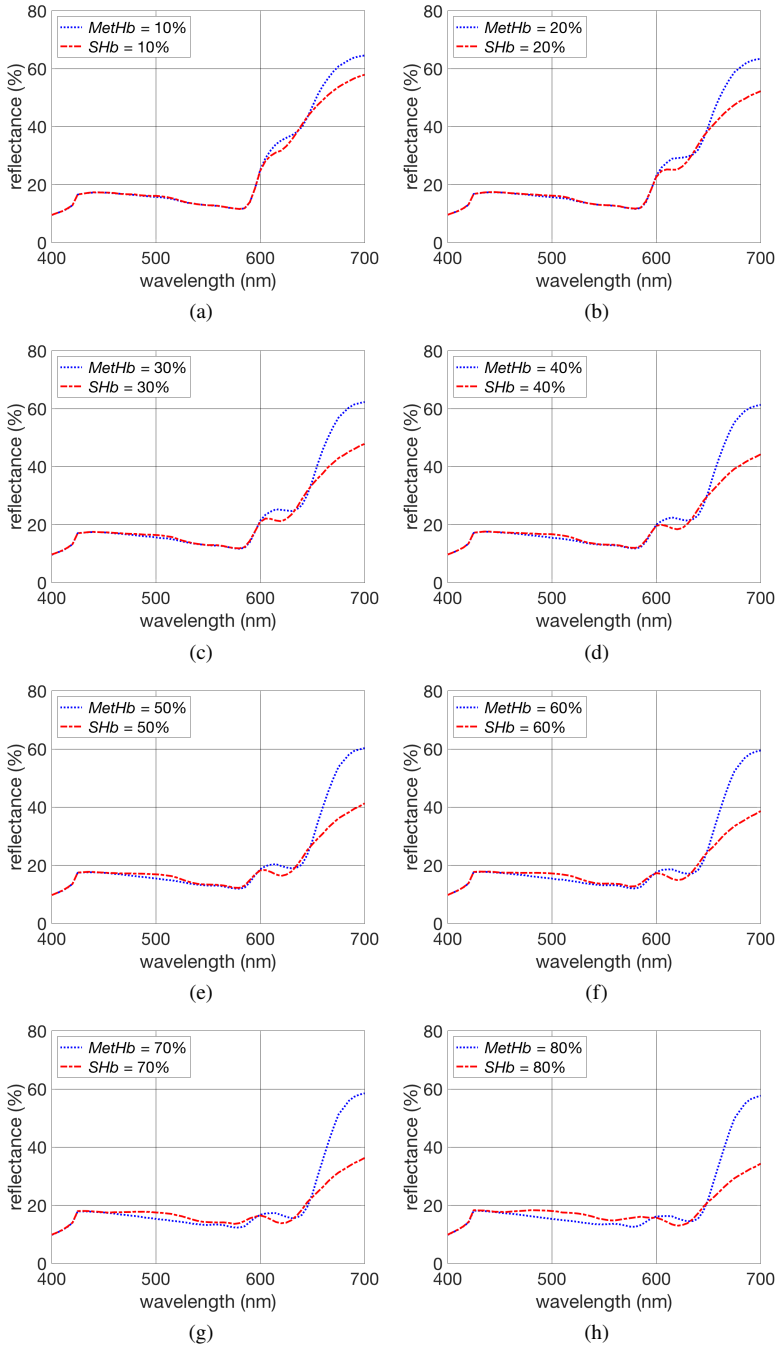

Fig. 5. Graphs depicting reflectance curves resulting from increasing amounts of methemoglobin (MetHb) and sulfhemoglobin (SHb) in a skin specimen characterized by a reticular blood content (v_{blood}^{rd}) equal to 10%. These curves were obtained using the HyLIoS [36] model and considering an angle of incidence equal to 15°. Each graph corresponds to a distinct severity level of methemoglobinemia and sulfhemoglobinemia: (a) 10%, (b) 20%, (c) 30%, (d) 40%, (e) 50%, (f) 60%, (g) 70% and (h) 80%. The concentrations of dysfunctional and functional hemoglobins associated with these levels are provided in Tables 2 and 3. The remaining parameters values used in the specimen's characterization are provided in Table 1.

Biomedical Optics EXPRESS

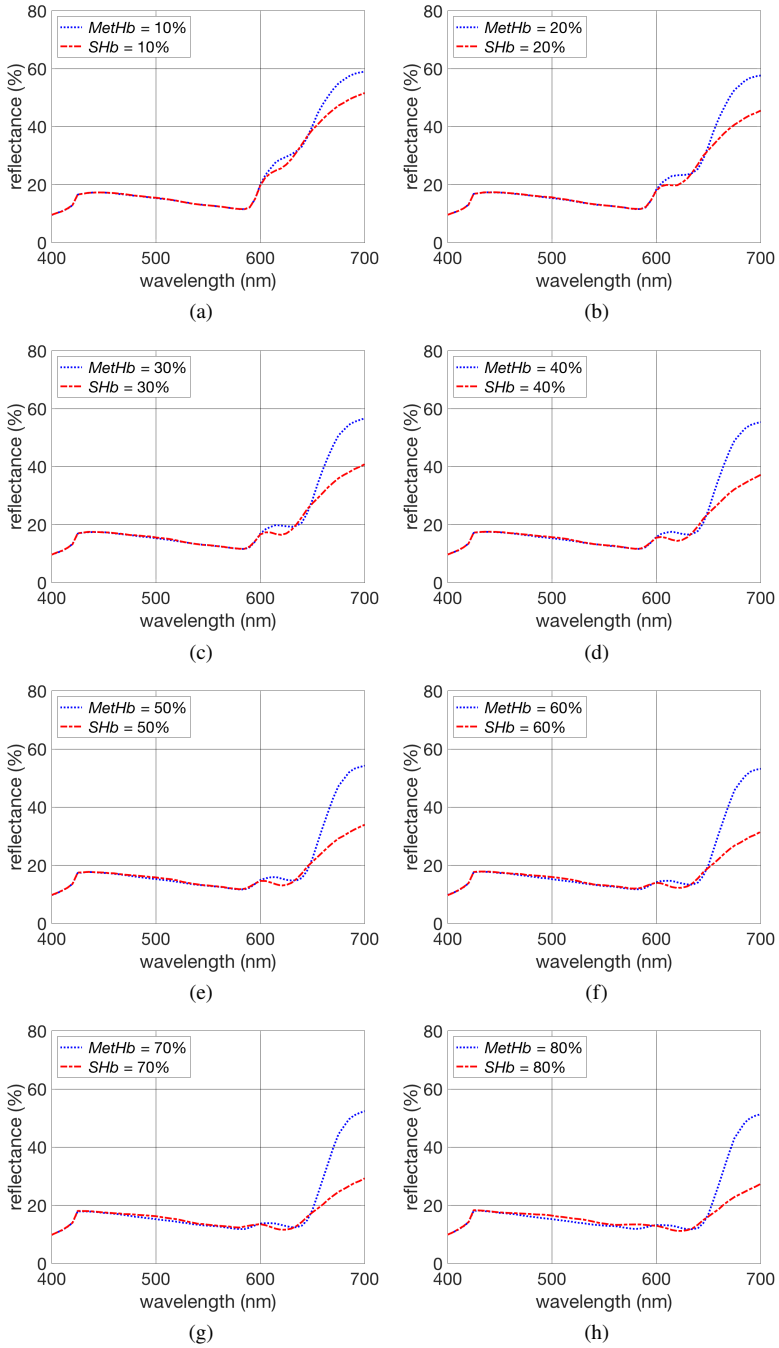

Fig. 6. Graphs depicting reflectance curves resulting from increasing amounts of methemoglobin (MetHb) and sulfhemoglobin (SHb) in a skin specimen characterized by a reticular blood content (v_{blood}^{rd}) equal to 15%. These curves were obtained using the HyLIoS [36] model and considering an angle of incidence equal to 15°. Each graph corresponds to a distinct severity level of methemoglobinemia and sulfhemoglobinemia: (a) 10%, (b) 20%, (c) 30%, (d) 40%, (e) 50%, (f) 60%, (g) 70% and (h) 80%. The concentrations of dysfunctional and functional hemoglobins associated with these levels are provided in Tables 2 and 3. The remaining parameters values used in the specimen's characterization are provided in Table 1.

Biomedical Optics EXPRESS

3.2. Cyanotic appearance changes

We remark that, as reported in the literature (*e.g.*, [4, 8, 10, 11]), skin spectral responses associated with methemoglobinemia and sulfhemoglobinemia lead to cyanotic skin appearances. One can expect that these appearances may vary according with the amounts of MetHb and SHb present in a patient's blood stream. In addition, it seems plausible that their characteristic chromatic attributes may be intensified as the blood content of the examined skin site increases. However, a quantitative investigation of the impact of these biophysical parameters on a patient's cyanotic appearance has not been performed to date.

In order to perform such an investigation, we employed the dysfunctional reflectance curves obtained from our *in silico* experiments (Section 3.1) to generate skin swatches depicting the appearance changes associated with these curves. In total, four sets of swatches were generated, one for each v^{rd}_{blood} value considered in our experiments, namely 2%, 5% 10% and 15%. These sets are presented in Figs. 7 to 10, respectively, along with CIELAB $\Delta E^{\star}_{ab}$ differences computed for each pair of swatches generated for the same abnormal amounts of MetHb and SHb.

As it can be observed in Fig. 7, an increase in the methemoglobinemia and sulfhemoglobinemia severity levels led to a pale appearance when we considered v^{rd}_{blood} equal to 2%. In addition, it also led to more distinguishable CIELAB $\Delta E^{\star}_{ab}$ differences between pairs of swatches generated considering the same amounts of MetHb and SHb.

When we employed higher values for v^{rd}_{blood}, the impact of increasing severity levels of methemoglobinemia and sulfhemoglobinemia on the swatches' appearance became more pronounced, with more characteristic cyanotic hues being elicited under these conditions. More specifically, one can observe a transition to red-purple (MetHb swatches) and grey (SHb swatches) hues in the 5% case (Fig. 8), to purple (MetHb swatches) and blue (SHb swatches) hues in the 10% case (Fig. 9), and to purple (MetHb swatches) and more saturated blue (SHb swatches) hues in the 15% case (Fig. 10).

The visual inspection of the swatches presented in Figs. 7 to 10 and the verification of their respective CIELAB $\Delta E^{\star}_{ab}$ differences reveal another relevant trend that can be summarized as follows. Although one can observe transitions to more characteristic cyanotic hues as higher v^{rd}_{blood} values are employed, the distinguishable CIELAB $\Delta E^{\star}_{ab}$ differences between pairs of swatches generated considering the same amounts of MetHb and SHb decreases. In practical terms, while a cyanotic appearance becomes more evident, the differentiation of their cause being an abnormal amount of MetHb or SHb becomes more problematic.

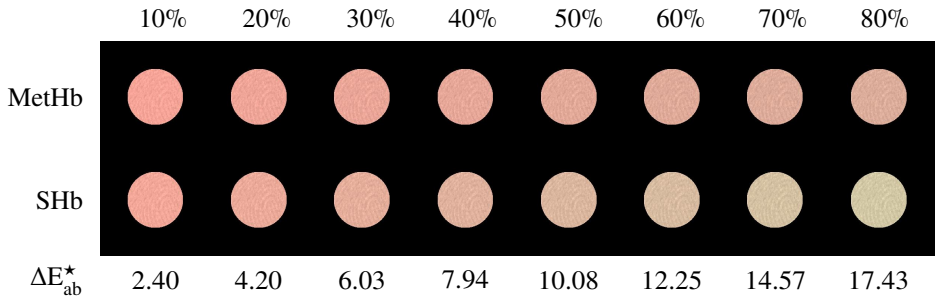

Fig. 7. Skin swatches generated using the dysfunctional reflectance curves provided in Fig. 3, which were obtained considering skin specimen characterized by a reticular blood content (v^{rd}_{blood}) equal to 2% and increasing amounts of methemoglobin (MetHb) and sulfhemoglobin (SHb), from 10% to 80%. The bottom row presents the the CIELAB $\Delta E^{\star}_{ab}$ differences for each pair of MetHb and SHb swatches.

Biomedical Optics EXPRESS

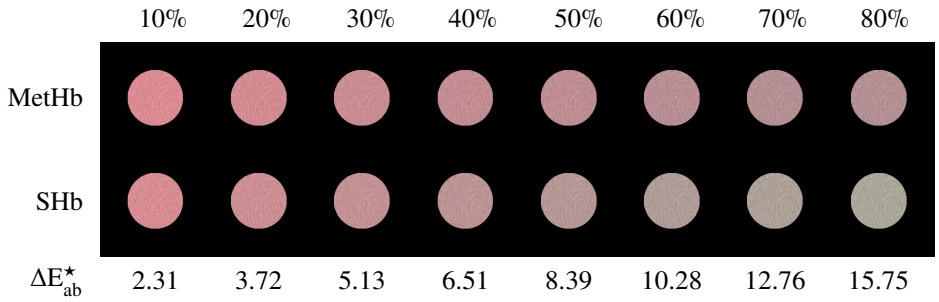

Fig. 8. Skin swatches generated using the dysfunctional reflectance curves provided in Fig. 4, which were obtained considering skin specimen characterized by a reticular blood content (v_{blood}^{rd}) equal to 5% and increasing amounts of methemoglobin (MetHb) and sulfhemoglobin (SHb), from 10% to 80%. The bottom row presents the the CIELAB $\Delta E_{ab}^{\star}$ differences for each pair of MetHb and SHb swatches.

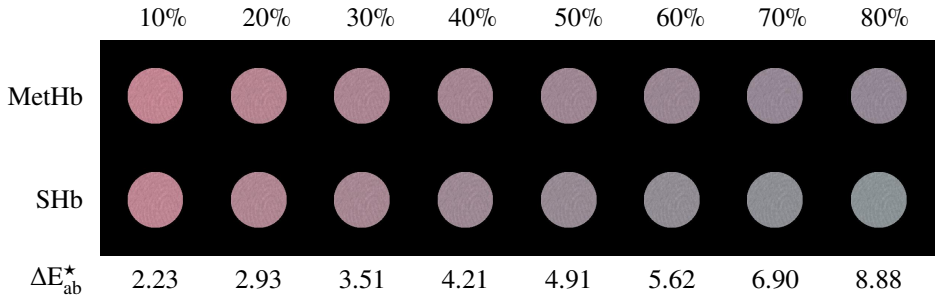

Fig. 9. Skin swatches generated using the dysfunctional reflectance curves provided in Fig. 5, which were obtained considering skin specimen characterized by a reticular blood content (v_{blood}^{rd}) equal to 10% and increasing amounts of methemoglobin (MetHb) and sulfhemoglobin (SHb), from 10% to 80%. The bottom row presents the the CIELAB $\Delta E_{ab}^{\star}$ differences for each pair of MetHb and SHb swatches.

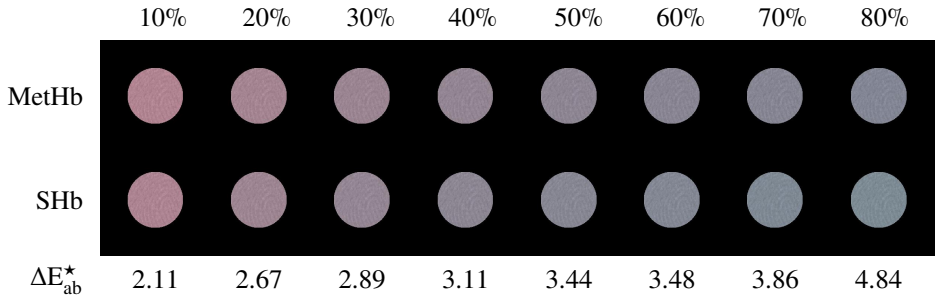

Fig. 10. Skin swatches generated using the dysfunctional reflectance curves provided in Fig. 6, which were obtained considering skin specimen characterized by a reticular blood content (v_{blood}^{rd}) equal to 15% and increasing amounts of methemoglobin (MetHb) and sulfhemoglobin (SHb), from 10% to 80%. The bottom row presents the the CIELAB $\Delta E_{ab}^{\star}$ differences for each pair of MetHb and SHb swatches.

Biomedical Optics EXPRESS

3.3. Proposed detection and differentiation protocol

The observations reported in Section 3.2 indicate that the visual assessment of a patient's cyanotic appearance is not a reliable candidate for the differentiation of methemoglobinemia and sulfhemoglobinemia. However, it can be used to assist the detection of these disorders. More specifically, once a cyanotic appearance has been observed in a patient, other more common cyanosis-eliciting conditions may be ruled out using diagnosis-aiding tools usually available to the medical staff. For example, as mentioned earlier, cyanosis is normally associated with the presence of high levels of deoxygenated hemoglobin in the dermal tissues [3]. Thus, if a patient with a high level (above 90%) of oxygenated (saturated) arterial hemoglobin develops a cyanotic appearance, it is likely that such an appearance is being elicited by a dyshemoglobinemia disorder [19]. We remark that oxygen saturation levels can be quickly measured using a pulse oximeter [7], an essential noninvasive device commonly available at the point of care of most medical settings.

After it has been detected that a patient is being subjected to either methemoglobinemia or sulfhemoglobinemia, the medical staff is left with the task of determining which of these conditions should be targeted for treatment. In order to accomplish this differentiation task in a painless and low-risk manner, ideally one would like to resort to a noninvasive procedure. Accordingly, we propose a procedure formulated using selected reflectance values obtained at the patient's cyanotic fingertips. In the remainder of this section, we outline this procedure and evaluate its effectiveness.

From fundamental calculus [98], we know that the curve representing a differentiable function $y = f(x)$ is concave up on the interval where y' is increasing, and concave down on a interval where y' is decreasing. Moreover, assuming that $y = f(x)$ is twice differentiable on an interval I, then the curve representing $f(x)$ over I is concave up if $y'' > 0$, and concave down if $y'' < 0$.

In our investigation, $f(x)$ corresponds to a modeled reflectance curve $\rho(\lambda)$, where λ represents the wavelength of interest. Upon a closer examination of the dysfunctional reflectance curves (Section 3.1) obtained from our *in silico* experiments, one can observe a markedly distinct behavior of the MetHb and SHb curves on the 605 to 635 *nm* interval. More specifically, while the curves obtained considering abnormal amounts of MetHb are concave down on this interval, the curves obtained considering abnormal amounts of SHb are concave up. These observations suggested that the sign of the second derivative of $\rho(\lambda)$ at the center (620 *nm*) of this interval can be used to differentiate reflectance curves resulting from the presence of abnormal amounts of MetHb and SHb in blood-perfused cutaneous tissues, with a '-' sign indicating the former and a '+' sign indicating the latter.

We note that the second derivative of a dysfunctional reflectance curve at 620 *nm* can be numerically computed using the following three point central difference formula [99]:

$$y''(620) = \frac{\rho(605) - 2\,\rho(620) + \rho(635)}{225}, \tag{2}$$

where $\rho(605)$, $\rho(620)$ and $\rho(635)$ correspond to reflectance values at 605, 620 and 635 nm, respectively.

Since, for differentiation purposes, we are only interested in the sign of the second derivative, the denominator in Eq. (2) can be omitted. Accordingly, we employed the following simplified formula to obtain the sign of the second derivative of the dysfunctional reflectance curves at 620 *nm*:

$$y''(620) = \rho(605) - 2\,\rho(620) + \rho(635). \tag{3}$$

Using Eq. (3) and $\rho(605)$, $\rho(620)$ and $\rho(635)$ values extracted from the dysfunctional reflectance curves presented in Section 3.1, we computed the signs of their respective second derivative at 620 *nm*. We remark that these curves were computed considering an angle of incidence equal to 15°. It is appropriate, however, to account for possible changes in the measurement conditions that

Biomedical Optics EXPRESS

can take place when one employs an actual optical device to collect reflectance data. For example, one can expect angular variations with respect to the angle of incidence due to slight curvature of the palmar fingertip. For this reason, we also repeated our *in silico* experiments considering angles of incidences equal to 0°, 30° and 45°, and extracted the $\rho(605)$, $\rho(620)$ and $\rho(635)$ values from the resulting dysfunctional reflectance curves, which are provided elsewhere [93] to conserve space. We then used Eq. (3) and these values to compute the signs of the second derivatives of these curves at 620 *nm*.

As it can be observed in the aggregated outcomes of these sign computations presented in Table 4, we were able to differentiate between methemoglobinemia and sulfhemoglobinemia in all tested instances. It is important to note that, although the signs depicted in Table 4 were obtained using $\rho(605)$, $\rho(620)$ and $\rho(635)$ values extracted from the resulting dysfunctional curves computed considering v^{rd}_{blood} equal to 2%, we have obtained [93] exactly the same signs for all tested instances when we used $\rho(605)$, $\rho(620)$ and $\rho(635)$ values extracted from dysfunctional curves computed considering v^{rd}_{blood} equal to 5%, 10% and 15%. For this reason, we present only one table to avoid repeating the same results four times.

Table 4. Second derivative signs (at 620 *nm*) of the dysfunctional reflectance curves resulting from our *in silico* experiments. The signs were computed using Eq. (3) and the reflectance values [93] extracted from these curves. The curves were computed using the HyLIoS model [36], the specimen's characterization parameter values presented in in Table 1, and considering four angles of incidence (0°, 15°, 30° and 45°) as well as distinct severity levels of methemoglobinemia and sulfhemoglobinemia (10% to 80%). The concentrations of dysfunctional (MetHb and SHb) and functional hemoglobins associated with these levels are provided in Tables 2 and 3. We note that we have obtained the signs above for all values of reticular blood content (v^{rd}_{blood}) considered in our investigation (2%, 5%, 10% and 15%) [93].

	MetHb				SHb			
	0°	15°	30°	45°	0°	15°	30°	45°
10%	–	–	–	–	+	+	+	+
20%	–	–	–	–	+	+	+	+
30%	–	–	–	–	+	+	+	+
40%	–	–	–	–	+	+	+	+
50%	–	–	–	–	+	+	+	+
60%	–	–	–	–	+	+	+	+
70%	–	–	–	–	+	+	+	+
80%	–	–	–	–	+	+	+	+

It is also worth noting that reflectance values measured using actual devices, such as spectrophotometers [94], may be susceptible to uncertainties associated with the device. A high precision device will have an uncertainty of ±0.001 or 0.1% [100]. A low precision device may have an uncertainty close to 1% [100, 101]. In order to assess the consistency of our observations with respect to these random fluctuations, we performed a set of simulations considering the presence of random noise (±1%) in our simulations.

Again, we were able to differentiate between methemoglobinemia and sulfhemoglobinemia in all tested instances [93]. Since the inclusion of tables containing all reflectance values used to obtain these results would take too much space, we also made them available elsewhere [93]. Nonetheless, for conciseness and verification purposes, we selected to provide here the reflectance values used to obtain the signs associated the most difficult differentiation instances found in our experiments. These instances, in which one can observe the closest proximity between MetHb and SHb in the selected spectral interval, correspond to the case where we set v^{rd}_{blood} equal to

Biomedical Optics EXPRESS

15%. The $\rho(605)$, $\rho(620)$ and $\rho(635)$ values extracted from the curves associated with these test instances are presented in Table 5, and the corresponding second derivative signed values (to enable the quantitative verification of the correctness of our calculations) computed using Eq. (3) are provided in Table 6.

Table 5. Reflectance values at 605, 620 and 635 *nm* extracted from dysfunctional curves computed using the HyLIoS model [36], the specimen's characterization parameter values presented in Table 1 and accounting for the presence of random noise (±1%) in our simulations. In the computation of these curves, we considered an angle of incidence of 15°, a reticular blood content (v_{blood}^{rd}) equal to 15% and distinct severity levels of methemoglobinemia and sulfhemoglobinemia (10% to 80%). The concentrations of dysfunctional (MetHb and SHb) and functional hemoglobins associated with these levels are provided in Tables 2 and 3.

	MetHb			SHb		
	605	620	635	605	620	635
10%	0.2320	0.2890	0.3141	0.2246	0.2578	0.3160
20%	0.2047	0.2330	0.2419	0.1940	0.1986	0.2427
30%	0.1828	0.1964	0.1973	0.1723	0.1634	0.2038
40%	0.1681	0.1707	0.1693	0.1574	0.1440	0.1724
50%	0.1566	0.1533	0.1477	0.1455	0.1308	0.1530
60%	0.1457	0.1415	0.1328	0.1378	0.1210	0.1393
70%	0.1374	0.1337	0.1248	0.1322	0.1150	0.1278
80%	0.1310	0.1256	0.1172	0.1263	0.1108	0.1208

Table 6. Second derivative values computed using the reflectance values provided in Table 5 and Eq. (3) for distinct severity levels of methemoglobinemia and sulfhemoglobinemia (10% to 80%). The concentrations of dysfunctional (MetHb and SHb) and functional hemoglobins associated with these levels are provided in Tables 2 and 3.

	10%	20%	30%	40%	50%	60%	70%	80%
MetHb	-0.0319	-0.0194	-0.0127	-0.0040	-0.0023	-0.0045	-0.0052	-0.0030
SHb	+0.0250	+0.0395	+0.0493	+0.0418	+0.0369	+0.0351	+0.0300	+0.0255

Previously, Baranoski et al. [26] have also proposed five-point and three-point central difference formulas for differentiating between methemoglobinemia and sulfhemoglobinemia. In their work, they were able to differentiate these disorders within a severity level range between 20% and 70% and considering only one value for the reticular blood content (5%). Using the proposed formula, we were able to differentiate these disorders within a broader severity level range (from 10% to 80%) and considering observed [48] physiological variations in the reticular blood content (from 2% to 15%). These observations indicate that the proposed three-point formula enables a wider range of sensitivity in the differentiation of methemoglobinemia and sulfhemoglobinemia without incurring in additional computational costs.

In summary, based on our *in silico* experimental findings, we proposed a protocol in which the patient's cyanotic appearance is employed to assist the detection of methemoglobinemia and sulfhemoglobinemia, and an optical procedure is used to differentiate these disorders. This procedure, in turn, would consist in the noninvasive measurement of three reflectance values at the patient's cyanotic fingertips followed by the sign computation using Eq. (3). These measurements would be performed at wavelengths within the visible (harmless) region of the light spectrum.

We note that the proposed differentiation procedure would require only three measurements, which could be obtained *in situ* (without the need, for example, of sending blood samples for

Biomedical Optics EXPRESS

analysis elsewhere) using a hand-held spectrophotometer, a relatively inexpensive device in comparison with co-oximeters and blood gas analysers. The operation of this device would require a minimum level of expertise. Alternatively, these measurements could be performed using a portable dedicated device with an embedded implementation of the proposed differentiation procedure, in a manner similar to the one employed to measure oxygen levels through pulse oximetry. This would reduce the operational overhead and the required level of user expertise even further. These deployment alternatives would certainly make the proposed differentiation procedure attractive for use at the point of care of low-resources medical settings.

Since other noninvasive optical monitoring procedures, such as pulse oximetry [7], also rely on light and skin interactions in the near-infrared domain, one might question the reason why we have not extended our investigation to this spectral domain. Although our *in silico* experimental framework can be used to obtain skin reflectance readings from the ultraviolet to the infrared domain, our investigation was centered at the visible domain for the following reasons. First, one of the focal points of our investigation, cyanosis, is directly associated with skin spectral responses in this spectral domain. Second, there is a relative scarcity of reliable data with respect to the extinction coefficients of MetHb and SHb outside the visible domain. The available data (*e.g.*, [52, 102]) indicates that the extinction coefficients of MetHb and SHb in the near-infrared domain may be one order of magnitude lower than their visible domain counterparts. This, in turn, suggests that the chances of finding significant spectral features to allow a reliable differentiation of methemoglobinemia and sulfhemoglobinemia are small in the near-infrared domain. Nonetheless, as reliable near-infrared extinction coefficient data for MetHb and SHb become available, it will be worthwhile to investigate the possibility of finding differentiation features for methemoglobinemia and sulfhemoglobinemia in this spectral domain as well.

4. Conclusion and future prospects

In this work, we have quantitatively examined the connection between the onset of cyanosis and distinct severity levels of methemoglobinemia and sulfhemoglobinemia. More specifically, we have demonstrated the impact of different amounts of MetHb and SHb on cyanotic chromatic attributes of a skin specimen also subject to variations on dermal blood content. We have also assessed the impact of these biophysical parameters on the specimen's spectral responses. Building on the findings derived from our *in silico* findings, we have proposed a cost-effective protocol for the detection and differentiation of methemoglobinemia and sulfhemoglobinemia. Our *in silico* evaluation of its effectiveness and sensitivity range suggests that it can represent a promising alternative to the technologies currently used in the detection and differentiation of these dyshemoglobinemia disorders.

It has been long recognized [33, 34] that *in silico* experiments performed through predictive computer simulations can be successfully employed to predict the quantitative behaviour of complex biological systems, to accelerate the hypothesis generation and validation cycles of biomedical research, notably those that cannot be performed using traditional "wet" laboratory technologies, and to drive new scientific investigations. It is important to keep in mind, however, that a computer simulation has a limited value if it is not being supported and verified against reliable data obtained through actual experiments performed either under *in vivo* and/or *in vitro* conditions. These experiments, for instance, could consist in reflectance measurements performed (*in vivo*) on a patient subjected to a dyshemoglobinemia disorder, followed by the collection blood samples to determine (*in vitro*) the MetHb and SHb levels in her/his blood stream. Furthermore, the pairing of computer simulations with actual experiments can contribute to a more straightforward translation of research outcomes obtained *in silico* to clinical practice.

Viewed in this context, our *in silico* findings and, in particular, the verification of the proposed protocol's effectiveness and sensitivity range would certainly benefit from confirmation through *in vivo* and/or *in vitro* experiments. We note, however, that the scarcity of *in vivo* and/or *in vitro*

Biomedical Optics EXPRESS

experiments involving the measurement of chromatic and spectral data associated with the onset of methemoglobinemia and sulfhemoglobinemia has motivated our use of an *in silico* approach in the first place. Moreover, we remark that our *in silico* experiments were performed using a first-principles model of light and skin interactions, whose predictive capabilities have been extensively evaluated in previous works [3, 36, 39–41]. Also, to the best of our knowledge, we have employed the most reliable supporting biophysical data, such as the spectral extinction coefficients for methemoglobin [103] and sulfhemoglobin [52], provided in the literature. Hence, we are confident that our findings can be corroborated by *in vivo* and/or *in vitro* obtained data as it becomes available.

As outlined above, the investigation presented in this paper also highlighted the need for databases depicting measured chromatic and spectral data obtained from skin specimens subject to pathological conditions, particularly those affecting the patients' appearance and posing a high risk of morbidity and mortality for them. In order to improve this situation, we believe that the biomedical community should support efforts directed to the creation of such databases. These should include, but not be limited to data related to dyshemoglobinemia disorders. These efforts would likely involve the establishment of synergistic collaborations between researchers and medical institutions interested in the development of new cost-effective technologies for the diagnosis and treatment of the targeted pathological conditions. Once these databases are created, it would be essential that they are made publicly accessible. In this way, they can be fully verified and employed by the entire biomedical community in a broad range of applications, from the reliable screening of serious medical conditions (*e.g.*, melanoma) to the efficacy and safety enhancement of skin care products (*e.g.*, sunscreens).

Funding

Natural Sciences and Research Council of Canada (NSERC) (238337).

Acknowledgments

The authors would like to thank the anonymous reviewers for their helpful suggestion.

Disclosures

The authors declare that there are no conflicts of interest related to this article.